Electronic Supplementary Material (ESI) for Sustainable Energy & Fuels.

Supplementary information

High-energy and high-power Zn-Ni flow batteries with semi-solid electrodes

Yun Guang Zhu§[a], Thaneer Malai Narayanan§[b], Michal Tulodziecki[a], Hernan Sanchez-Casalongue[d], Quinn Horn[d], Laura Meda[e], Yang Yu[c], Jame Sun[b], Tom Regier[f], Gareth H. McKinley*[b], Yang Shao-Horn*[abc]

[a] Research Laboratory of Electronics, Massachusetts Institute of Technology, 77 Massachusetts Avenue, Cambridge, USA

[b] Department of Mechanical Engineering, Massachusetts Institute of Technology, 77 Massachusetts Avenue, Cambridge, USA

[c] Department of Material Science and Engineering, Massachusetts Institute of Technology, 77 Massachusetts Avenue, Cambridge, USA

[d] Materials & Corrosion Engineering, 1075 Worcester St, Natick, MA 01760

[e] Dipart. Chimica-Fisica, Istituto Eni Donegani, Centro Recerche per Rinnovabili e Ambiente, Italy

[f] Canadian Light Source Inc., Saskatoon, Saskatchewan S7N 0X4, Canada

§ These authors contributed equally.

Experimental section

Materials

Potassium hydroxide (KOH, 99%, VRM) was used for electrolyte preparation. Carbopol© (Carbopol© 940 NF polymer, Lubrizol, USA) was used as a gelling agent to stabilize the suspension. Zinc oxide (ZnO, 99%, Sigma-Aldrich) and alloyed zinc powder (EverZinc, Belgium) were used for anolyte preparation, where Zn served as the conductive additive. Nickel hydroxide ($Ni(OH)_2$, 98%, Pred Materials, USA and Kansai Catalyst Co. Ltd., Japan) and acetylene black (AB, Chevron, USA) were used for catholyte preparation, where AB served as the conductive additive. Cobalt oxide (CoO, 99.995%, Fisher Scientific) was also used to further enhance the conductivity of $Ni(OH)_2$ as suggested by Leger et al. [1].

Anolyte preparation

30 w% KOH solution was prepared by dissolving 5.36 g of KOH pellets in 12.5 ml deionized water. Then, 0.57 g of ZnO was added to the above solution and stirred using a magnetic stirrer for 5 hours to be dissolved as zincate ions. After that, 0.18 g of Carbopol© was added to the above solution and mixed with a planetary mixer (Thinky AR-100, Japan). The electrolyte gel was kept at rest for 12 hours to allow swelling of Carbopol© microgels. The electrolyte gel was then remixed before adding ZnO at amounts as described in Table 1 and mixed again after. Finally, Zn was added to the suspension and mixed at 2000 rpm for 6 minutes. All other mixing was performed at 2000 rpm and 12 minutes unless stated otherwise.

Catholyte preparation

30 w% KOH solution (7 M KOH solution) was prepared by dissolving 5.36 g of KOH pellets in 12.5 ml deionized water. Then, 0.18 g of Carbopol© was added to the above solution and mixed with a planetary mixer (Thinky AR-100, Japan). The electrolyte gel was kept at rest for 12 hours to allow swelling of Carbopol© microgels. The electrolyte gel was then remixed before adding AB at amounts as described in Table S3 & S4 and mixed again after. For the preparation of active suspension, $Ni(OH)_2$ + CoO (100/5 by weight) powder mixture was ground with AB prior to adding to the electrolyte gel at $Ni(OH)_2$ amounts described in Table S4. All mixing was performed at 2000 rpm for 12 minutes.

Table S1. Zn conductive suspension compositions

30 w% KOH solution with 0.5 M ZnO (vol%)	**Carbopol 940 (vol%)**	**Zn particles (vol%)**
94.7	1.1	4.2
93.4	1.1	5.5
91.9	1.1	7.0
90.3	1.0	8.7
88.5	1.0	10.5
84.1	1.0	15.0
76.1	0.9	23.1

Table S2. ZnO/Zn semi-solid electrode compositions

30 w% KOH solution with 0.5 M ZnO (vol%)	Carbopol 940 (vol%)	Zn particles (vol%)	ZnO (vol%)
76.1	0.9	23.1	–
75.1	0.9	22.9	1.1
73.5	0.9	22.5	3.2
72.0	0.8	22.0	5.2
69.8	0.8	21.3	8.1

Table S3. Acetylene black (AB) conductive suspension compositions

30 w% KOH solution (vol%)	Carbopol 940 (vol%)	AB (vol%)
98.3	0.9	0.8
97.4	0.9	1.7
96.6	0.9	2.5
95.7	0.9	3.4
94.8	0.9	4.3
93.9	0.9	5.2
93.4	0.9	5.7
93.0	0.9	6.2
92.5	0.9	6.7

Table S4. $Ni(OH)_2$/AB semi-solid electrodes compositions

30 w% KOH solution (vol%)	**Carbopol 940 (vol%)**	**AB (vol%)**	**$Ni(OH)_2$ (vol%)**
92.4	0.9	6.1	0.7
91.4	0.8	6.1	1.7
89.7	0.8	5.9	3.5
85.9	0.8	5.7	7.6
83.7	0.8	5.5	10.0
81.3	0.7	5.4	12.5

Rheological property characterization

Rheological measurements of the suspensions were performed on an AR-G2 controlled stresss rheometer (TA Instruments) using a 40 mm plate-plate geometry. To prevent wall slip, the plates were covered with adhesive-backed lapping film containing 30 μm diamond abrasive for $Ni(OH)_2$/AB suspension and adhesive-backed sandpaper with 100 μm silicon carbide abrasive for the ZnO/Zn suspension. The abrasive particle sizes were chosen to match the average size of the $Ni(OH)_2$ and Zn particles respectively. A gap of 1200 μm was used for all measurements unless stated otherwise. Decreasing step shear-rate-controlled viscometry was performed to measure the flow curve. For AB, ZnO/Zn, $Ni(OH)_2$/AB suspensions, each shear rate was held constant for 30 s before measuring the stress. The same procedure was repeated three times with fresh samples to obtain the average stress at a given shear rate.

Zn-Ni semi-solid static and flow cells

A closed static cell was designed to test the intrinsic electrochemical performance of the suspensions in static mode. A milled bipolar graphite well (Fuel Cell Store, USA) serves as a catholyte current collector and a brass plate (McMaster-Carr, USA) as an anolyte current collector. The catholyte and anolyte were separated by a piece of Celgard© 3501 separator. The cell was sealed with a natural rubber O-ring to prevent evaporation of electrolyte. The schematic of the static cell is shown in Figure 4a. The dimensions of a single electrode well are Φ 1.2 cm × H 0.2 cm. The dimensions of the fully assembled cell are Φ 5.8 cm × H 2.8 cm, including current collector, spacer, separator and stainless steel case.

The flow cell was used to test the applicability of the suspensions for flow battery. The same current collectors as were used for the closed-cell tests were employed. The flow cell spacer was 3-D printed using FormLabs© Clear resin. The catholyte and anolyte were separated by a piece of Celgard© 3501 separator. The schematic and photograph of the flow cell is shown in Figure 5a and b. The dimensions of a single channel (L × W × H) are 4 × 0.3 × 0.3 cm^3. The dimensions of the fully assembled cell (L × W × H) are 8.75 × 3.75 × 2 cm^3, including current collector, spacer, separator and acrylic cover. Suspensions were pumped into the flow cell using a syringe pump at 0.2 ml/min. Galvanostatic charge-discharge was performed in static mode. The capacities of excess ZnO/Zn anolytes used in the static and flow cells was >2 times higher than these of $Ni(OH)_2$ catholytes.

Electrochemical characterization

The cyclic voltammetry (CV) measurements were conducted through a three-electrode system with 30 w% KOH electrolyte. The reference electrode was Hg/HgO and the counter electrode was made of Ni foam. The preparation of Zn/ZnO working electrode is described as following: 0.7 g ZnO, 0.05 g Bi_2O_3, 0.1 g AB, 0.05 g alloyed Zn particles, and 0.1 g polyvinylidene fluoride binder (PVDF, Kynar HSV 900, Arkema, France) were ground for 30 min. Then, 1.5 ml of N-Methyl-2-pyrrolidone (NMP) was added to the above mixture and stirred using a magnetic stirrer for 12 h. Thereafter, the paste was painted on the Ni foam electrode and dried at 110 ^{o}C under vacuum for 5 h. The preparation of $Ni(OH)_2$ working electrode is described as following: 0.6 g of $Ni(OH)_2$, 0.25 g of AB, and 0.15 g of PVDF were ground for 30 min. After that, 2.0 ml of NMP was added to the above mixture and stirred for 12 h. Then, the paste was painted on the Ni foam and dried at 110 ^{o}C under vacuum for 5 h. The working electrodes (1×2 cm^2) were compressed under 5 tons of static pressure for 30 s prior to use.

The conductivity of the suspensions was measured using home-made conductivity cells. The suspensions were filled in rubber gasket between two blocking electrodes. Impervious graphite plates (Fuel Cell Store, USA) and brass plates (McMaster, USA) were used as electrodes for catholytes and anolytes, respectively. The geometrical area was 0.79 cm^2 and thickness of the gasket was 0.17 cm. The resistance, R of the suspension was determined by Linear Sweep Voltammetry (LSV). Conductivity was then calculated using the following equation.

$$\sigma_e = \frac{1}{R}\left(\frac{t}{A_{geo}}\right) \tag{1}$$

where t is the thickness of the gasket and A_{geo} is the geometrical area of the cell.

The galvanostatic charge-discharge measurements and electrochemical impedance spectroscopy (EIS) were conducted using static cells and flow cells. For galvanostatic charge-discharge tests, an initial activation process was applied[1]. The Zn-Ni static cells were charged and discharged in the activation cycle (one cycle) with a current density of 1 mA/cm^2_{geo}, and the charging capacity was set as 120% SOC based on $Ni(OH)_2$ and the discharge cut-off voltage is 0.8 V. After this activation process, the Zn-Ni cells were tested based on different current densities and different SOCs. The galvanostatic current densities were varied from 1 to 50 mA/cm_{geo}^2. Charge capacity was limited from 40 to 100 % status of charge (SOC) based on 1 electron transfer of $Ni(OH)_2$. The weight of the suspension was measured before cell assembly. EIS measurements were performed for frequencies 0.01 Hz to 1 MHz and a voltage amplitude of 10 mV.

Materials characterization

$Ni(OH)_2$ particles were collected for X-ray diffraction (XRD, Bruker) and scanning electronic microscopy (SEM, Zeiss Merlin) for detection of phases and morphologies, before and after galvanostatic cycling. The semi-solid electrode was washed by DI water 3 times, collected through centrifugation and dried in a vacuum oven at 70 ^{o}C overnight before above measurements.

Ex-situ L-edge X-ray absorption near-edge structure (XANES) measurements were performed at the Canadian Light Source (CLS). The Ni L3/2 edge XANES were obtained at the undulator-based Spherical Grating Monochromator (SGM) beamline. The powders were fixed with carbon adhesive tape on the aluminium substrate. The $Ni(OH)_2$ samples were chosen under the different status of charge after washing and drying as described above. 10 scans of Ni L-edge XANES for each sample were collected and averaged. The step size of the XANES measurement is 0.1 eV.

Micro X-ray computed tomography measurements

X-ray Computed tomography (CT) scans were performed utilizing a Nikon XTH 225 ST system at Exponent's Natick, MA facility. X-rays were generated in a microfocus tube and data was collected utilizing a Perkin Elmer 1621 EHS Detector. For the $Ni(OH)_2$ particles, X-rays were generated at a voltage of 150 kV and a current of 0.040 mA, with no filter being applied. Data was collected at a 1.415 s exposure. The scan was reconstructed with a beam hardening parameter of 1 utilizing Nikon's XTEKCT software, resulting in a voxel size of approximately 4 microns. For the Zn-ZnO anolyte, X-rays were generated at a voltage of 200 kV and a current of 0.048 mA, with no filter being applied. Data was collected at a 1.000 s exposure. The scan was reconstructed with a beam hardening parameter of 1 utilizing Nikon's XTEKCT software, resulting in a voxel size of approximately 7 microns.

Selection of polymer additive to improve stability of the semi-solid electrode

Hydrophobic functional groups on the carbon black surface typically prevent stable dispersion of carbon black aggregates in an aqueous solvent. As demonstrated by Parant *et al.*[2], polysaccharide-based polymers (e.g. gum Arabic) are usually added to stabilize dispersions of acetylene black inks. Adsorption of the polymer chains on the carbon black surface alters the surface charge of the carbon black enabling stable dispersion of the fractal carbon aggregates in aqueous solvents. However, such a technique did not work in alkaline solutions as the polysaccharides undergo hydrolysis in a concentrated alkaline environment.[3] Obvious discoloration of xanthan gum solution from clear to brown solution was observed when dispersed in 7M KOH. Therefore, we utilized an alkaline-stable polymer-based microgel (Carbopol©) to "trap" (stably suspend) both acetylene black and $Ni(OH)_2$ particles in the catholyte slurries, and both Zn and ZnO particles in the anolyte slurries. A similar technique has been used to stabilize the Zn electrode in commercial alkaline primary batteries.[4]

Estimation of mechanical energy dissipated during pumping

Flow behavior of semi-solid electrode gels can be analyzed simply using the Bingham model for yield stress fluids. Using the Bingham constitutive equation, the gel behaves like a rigid solid below the yield stress ($\tau < \tau_y$) and flows like a Newtonian liquid above the yield stress ($\tau > \tau_y$). The energy loss ($\varepsilon_{\text{pump}}$) due to pumping for channel flow of Bingham model-fluid can be simplified using Equation 1 and 2[5]

$$\varepsilon_{pump}(\%) = \frac{\Delta P}{E_{density}} \times 100\% \qquad (1)$$

$$\Delta P \approx \frac{2\tau_y}{H} L = \frac{2\tau_y P_{output}}{H\ P_{density}} \left(\frac{1}{wn}\right) \qquad (2)$$

where n is the number of parallel channels, L, H, and w are the length, thickness and width of the channels, respectively. Here $E_{density}$ is the energy density of the suspension (in $Wh/m^3_{\text{catholyte}}$), P_{output} is the required power output (in W) and $P_{density}$ is the power density obtainable from the stack performance (in W/m^2). For this analysis, the channel dimensions were assumed to be similar to conventional flow battery stack: the channel width w was set to 30 cm, the number of parallel channels n was set at 30 to obtain similar voltages (~30 to 40 V) as a typical stack. Furthermore, for the SSFB design calculation, the thickness was set at 2 mm, and the electrode was assumed to flow through the channel only once.[5-7] This flow is also assumed to be continuous at a very low flow rate (high Bingham number, Bn)[7] such that the electrochemical performance is identical to static cell performance. The length of a flow channel was chosen such that the stack power output P_{output} meets the 1 kW requirement. The energy density $E_{density}$ of the flowable electrode was set at a nominal value of 100 $\mathrm{Wh/L_{catholyte}}$ (100,000 $\mathrm{Wh/\ m^3_{catholyte}}$). Although the literature compared in Figure 1 (main text) has varied energy density values from about 45 $\mathrm{Wh/L_{catholyte}}$ to 200 $\mathrm{Wh/L_{catholyte}}$, the nominal value selected here is appropriate to give an approximate order of magnitude of energy dissipated during pumping. The power density $P_{density}$ is the product of average discharge voltage (V) and maximum current density ($\mathrm{W/m^2_{geo}}$) reported.

Additional experimental results

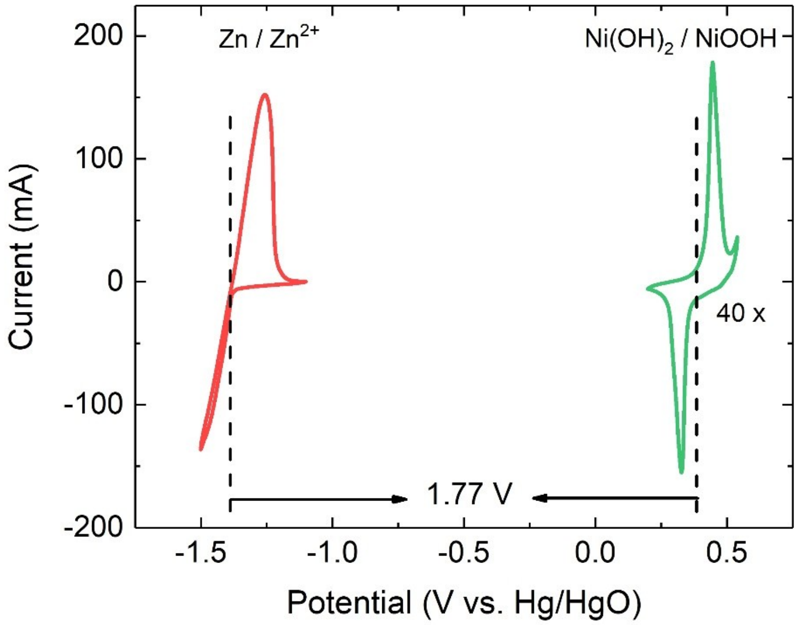

Figure S1. (a) CV curves of ZnO and $Ni(OH)_2$ in 30 w% KOH electrolyte. The working electrode is ZnO or $Ni(OH)_2$ on Ni foam. The reference electrode is Hg/HgO (4.4 M NaOH solution). The counter electrode is Ni foam. The scan rates are 1 mV/s for ZnO and 0.1 mV/s for $Ni(OH)_2$ (b) The schematic structure of Zn-Ni semi-solid flow battery, containing two energy storage tanks, a cell stack separated by a porous membrane, and active semi-solid electrolytes. The redox potential of Hg/HgO is 0.098 V vs SHE.

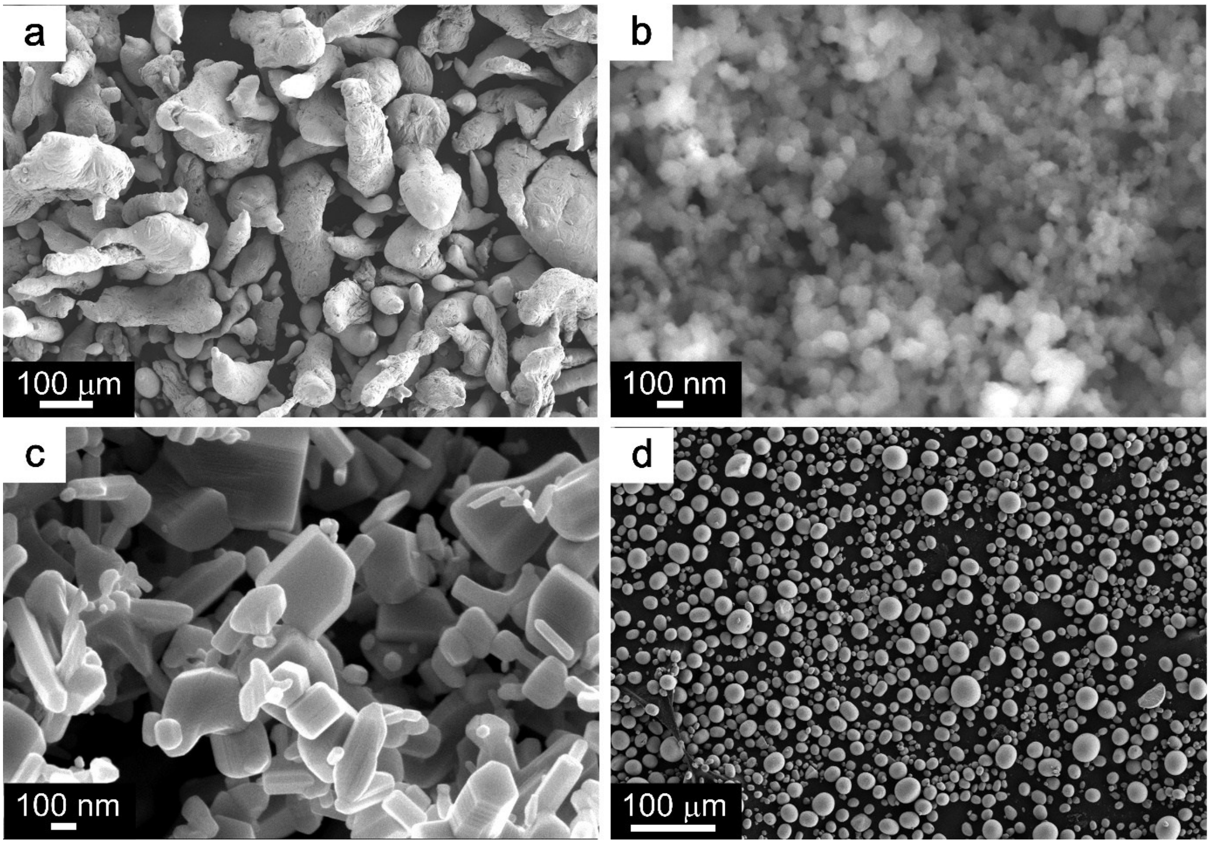

Figure S2. SEM images of Zn (a), AB (b), ZnO (c), and $Ni(OH)_2$ (d) used for suspension preparation.

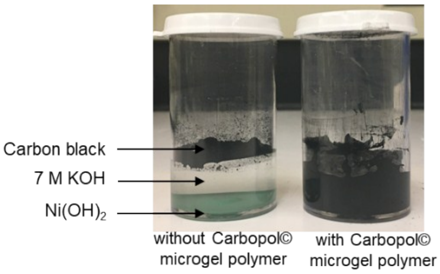

Figure S3. Phase separation of catholyte can be prevented by dispersing Carbopol© microgel polymer within the electrolyte. The Carbopol© microgel particles form an independent stress-bearing network[8] to prevent solid particle sedimentation whilst at the same time preventing irreversible aggregation of the attractive carbon black dispersion[9].

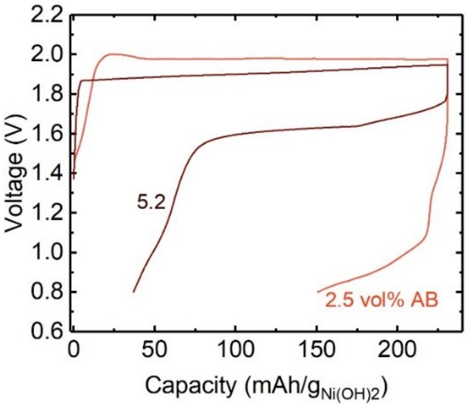

Figure S4. The charge/discharge profiles of Zn-Ni semi-solid cells are affected by AB concentration (2.5, and 5.2 vol%) in $Ni(OH)_2$ catholyte. Zn-Ni semi-solid static cells contain ZnO/Zn anolyte (3.2 vol% of ZnO and 22.5 vol% of Zn), and different catholytes containing 0.7 vol% $Ni(OH)_2$ and two different concentrations of AB indicated above.

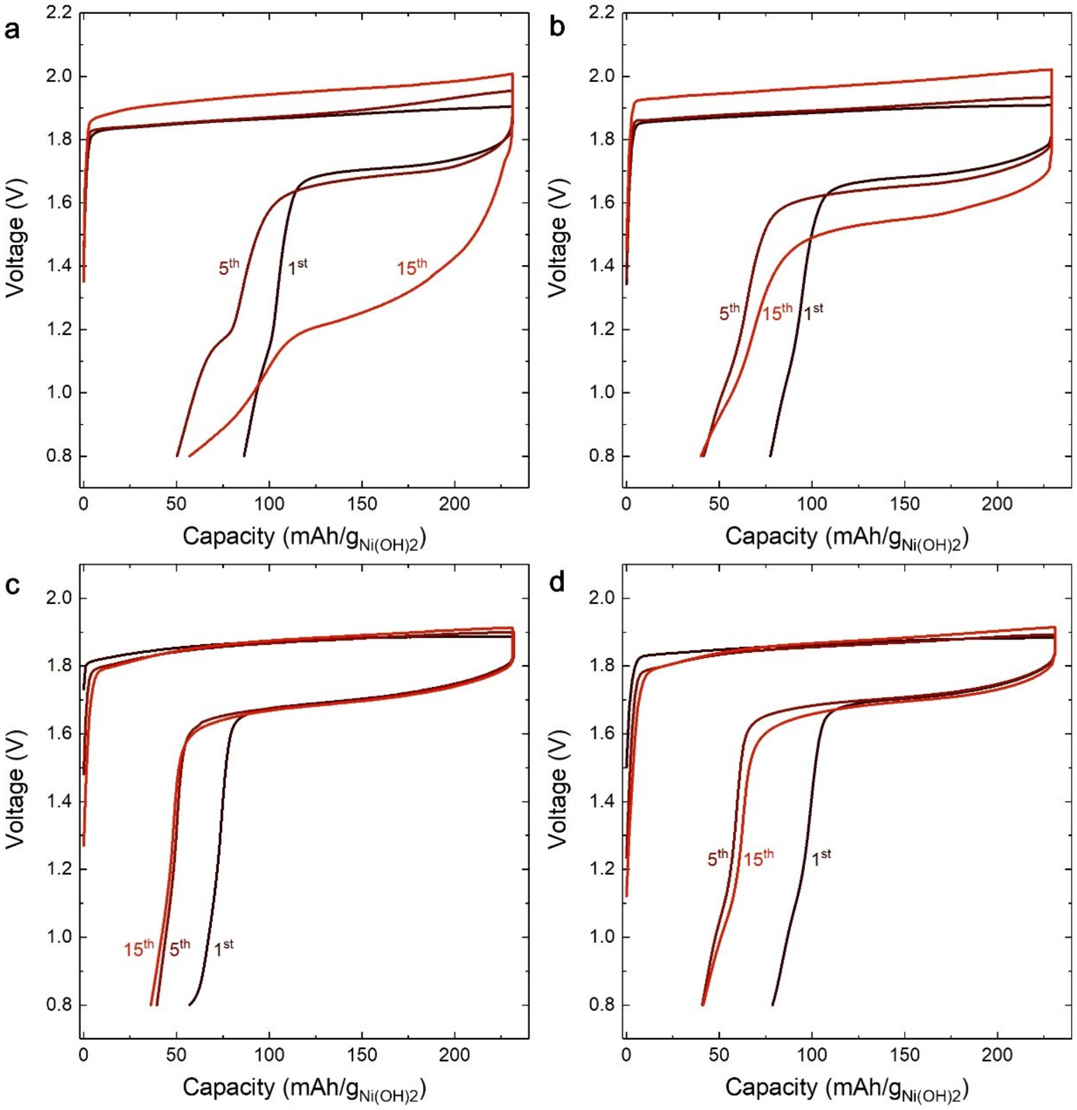

Figure S5. The charge-discharge tests of Zn-Ni semi-solid static cells with 3.2 vol% of ZnO anolyte and 0.7 vol% of $Ni(OH)_2$ catholyte with different concentrations of AB. The applied current is 2 mA/cm^2_{geo} and the operating voltage range is from 0.8 to 2.1 V. The AB volume fractions are 4.3 vol% (a), 5.2 vol% (b), 5.7 vol% (c), and 6.2 vol% (d), respectively. Each battery was tested for 15 cycles. The charge capacity is limited to 80% SOC (231 $mAh/g_{Ni(OH)2}$) of catholyte. All above charge/discharge curves were collected after one activation cycle with 120% SOC as described in the experimental section.

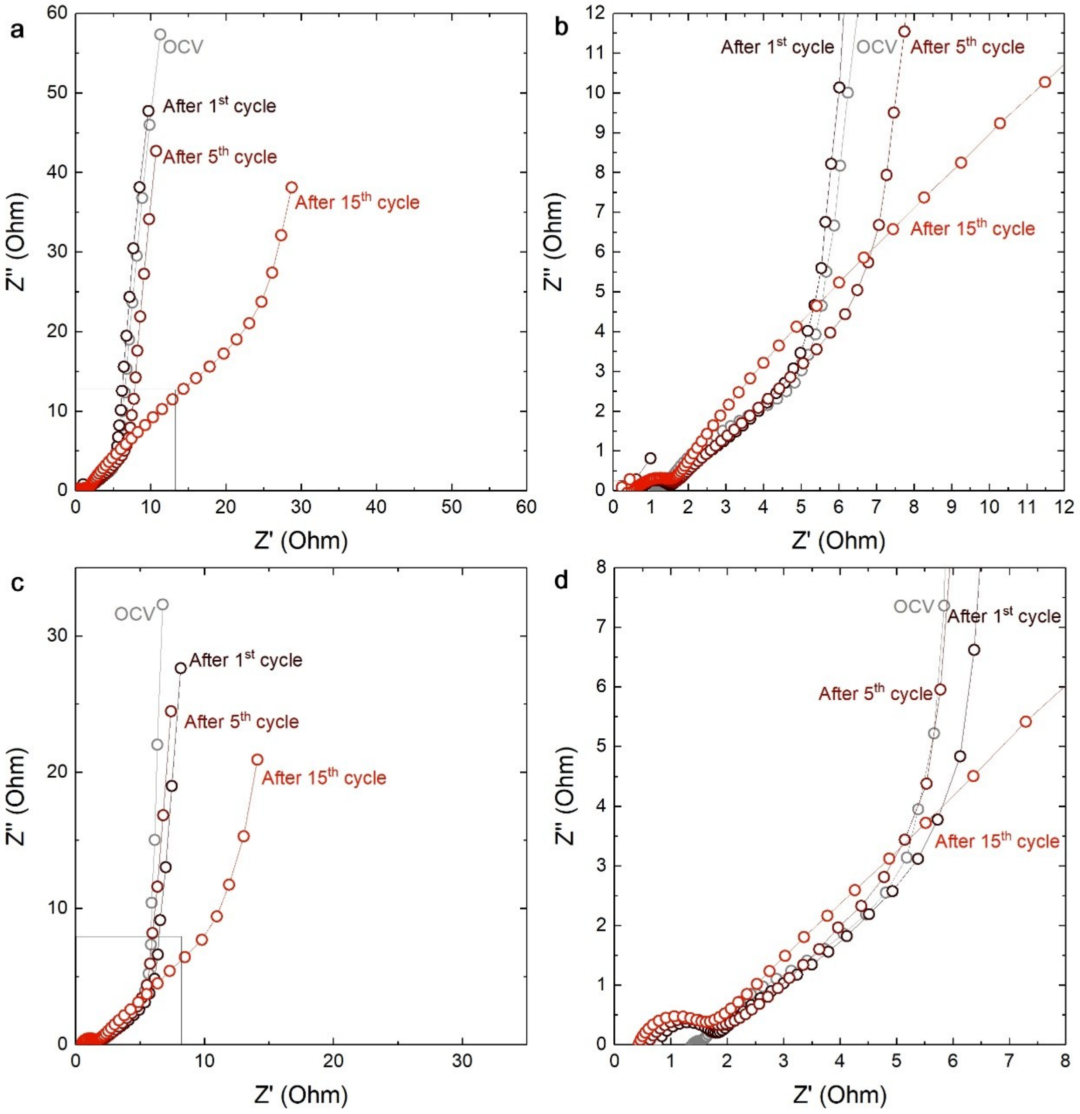

Figure S6. The evolution of impedance with cycling number for Zn-Ni semi-solid cells (with the charge-discharge curves shown in Figure S4a and S4d) containing 3.2 vol% of ZnO anolyte and 0.7 vol% $Ni(OH)_2$ catholyte with, respectively 4.3% (a and b) and 6.2 vol% (c and d) of acetylene black (AB) added. Data within the grey rectangles marked on the left are enlarged and shown on the right. Note: OCV is the abbreviation of open circuit voltage.

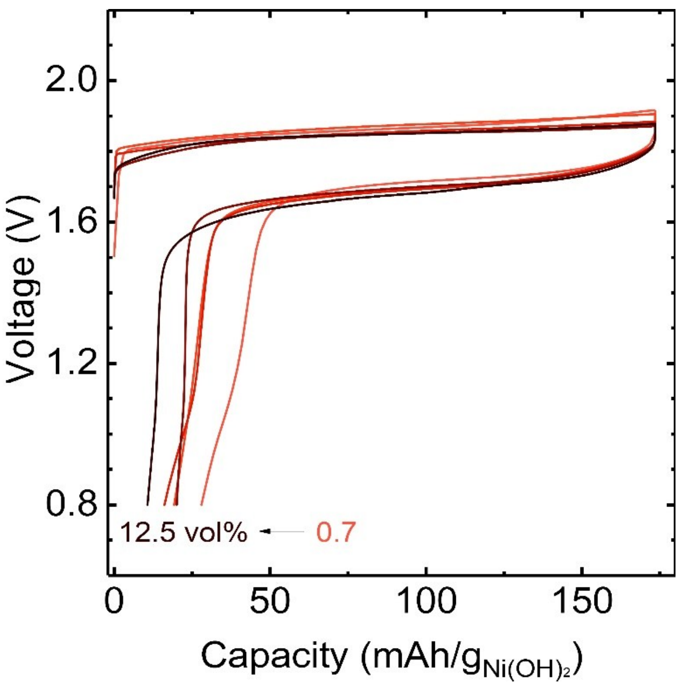

Figure S7. The charge-discharge profiles of Zn-Ni semi-solid static cells with anolyte of 5.2 vol% of ZnO and different catholytes containing 5.4-6.1 vol% AB and various volume percentages of Ni(OH)2 (0.7, 1.7, 3.5, 7.6, and 12.5 vol%). The applied current was 2 mA/cm$^2_{geo.}$ and the charge capacity was set as 60% SOC based on catholyte. All above charge/discharge curves were collected after one activation cycle with 120% SOC as described in the experimental section.

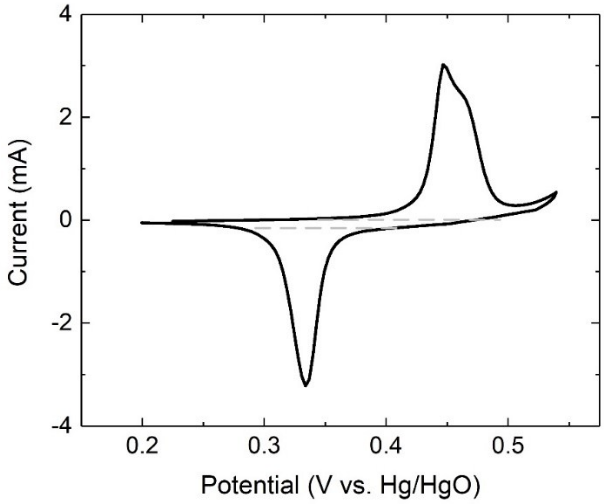

Figure S8. CV curve of $Ni(OH)_2$ in 30 w% KOH electrolyte after activation process[10]. The working electrode is $Ni(OH)_2$ on Ni foam. The reference electrode is Hg/HgO (4.4 M NaOH solution). The counter electrode is Ni foam. The scan rate is 0.1 mV/s. The operating potential range is from 0.2 to 0.54 V vs. Hg/HgO.

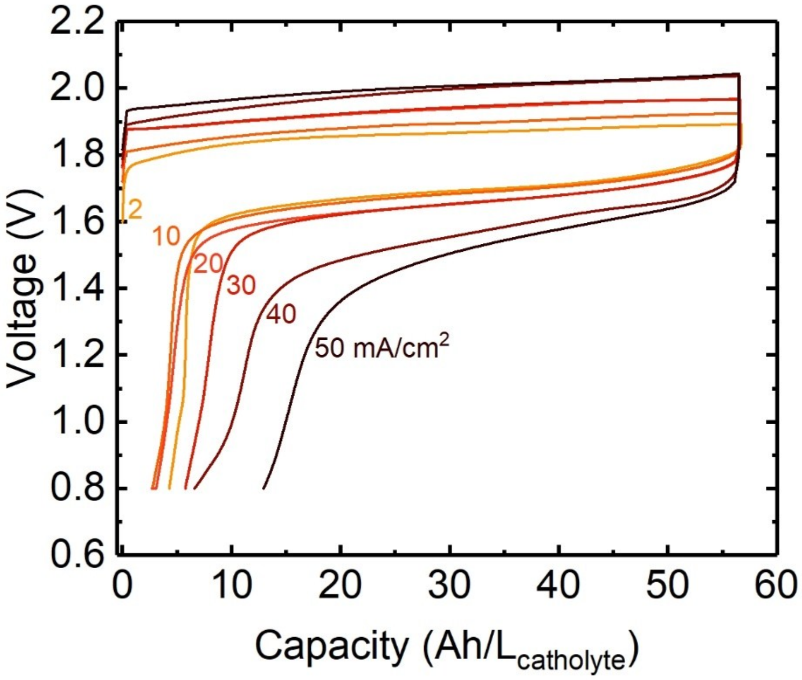

Figure S9. The rate capability of the semi-solid static cell with 12.5 vol% of $Ni(OH)_2$ + 5.4 vol% AB catholyte and 5.2 vol% ZnO + 22.0 vol% Zn anolyte. The charge capacity was set as 40% SOC based on catholyte (116 mAh/$g_{Ni(OH)2}$) with current densities of 2, 10, 20, 30, 40, 50 mA/cm_{geo}^2. All above charge/discharge curves were collected after one activation cycle with 120% SOC as described in the experimental section.

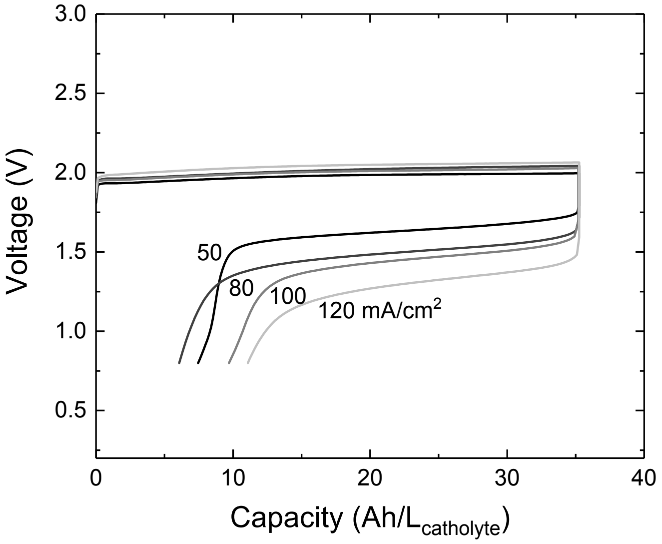

Figure S10. The high-power density achieved in semi-solid static cells with 5.2 vol% ZnO + 22.0 vol% Zn anolyte and 7.6 vol% of $Ni(OH)_2$ + 5.7 vol% of AB catholyte. The charge current density is 50 mA/cm^2 and discharge current densities are 50, 80, 100 and 120 mA/cm^2. The charge capacity was set as 40% $SOC_{Ni(OH)2}$. The operating voltage window is from 2.1 to 0.8 V. The Cu mesh (100 × 100) was added in the anode for even distribution of Zn plating during the charging process. All above charge/discharge curves were collected after one activation cycle with 120% SOC as described in the experimental section.

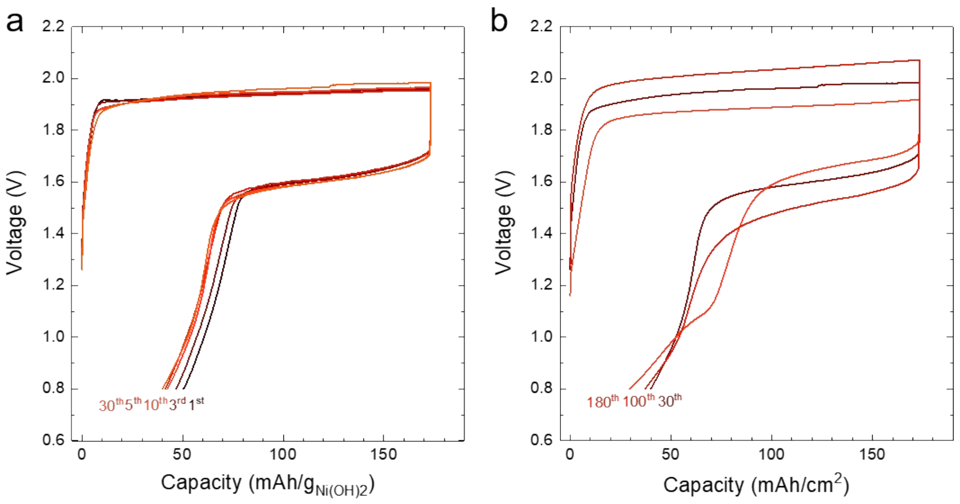

Figure S11. The charge-discharge profiles of Zn-Ni static cell (1st, 3rd, 5th, 10th, and 30th cycle in (a) and 30th, 100th, and 180th cycle in (b)) for cycling stability measurement. The cycling stability measurement of Zn-Ni semi-solid cell with 0.7 vol% $Ni(OH)_2$ + 6.1 vol% AB catholyte and 5.2 vol% ZnO + 22.5 vol% Zn anolyte. The applied current was 1 mA/cm$^2_{geo.}$. The charge capacity was limited 60 % SOC. The charge/discharge data was collected after one activation cycle with 120% SOC as described in the experimental section.

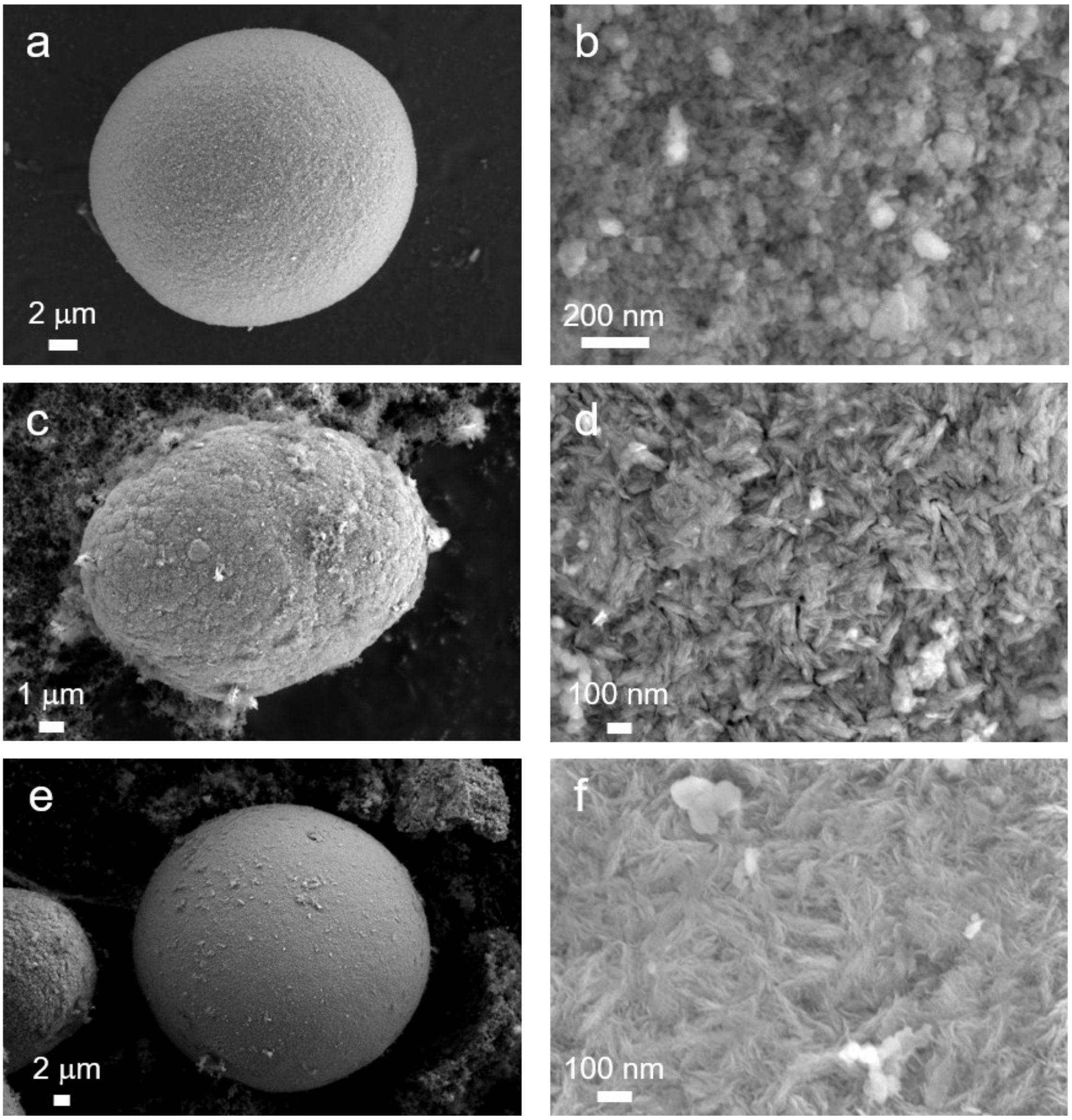

Figure S12. The $Ni(OH)_2$ sphere particles from catholyte before (a, b) and after 20 (c, d) 180 charge and discharge cycles (e, f). The cycling stability measurement of Zn-Ni semi-solid cell with 0.7 vol% $Ni(OH)_2$ + 6.1 vol% AB catholyte and 5.2 vol% ZnO + 22.5 vol% Zn anolyte. The applied current was 1 $mA/cm^2_{geo.}$. The charge capacity was limited 60 % SOC. The cycling performance is referred to Figure 4f in the main text.

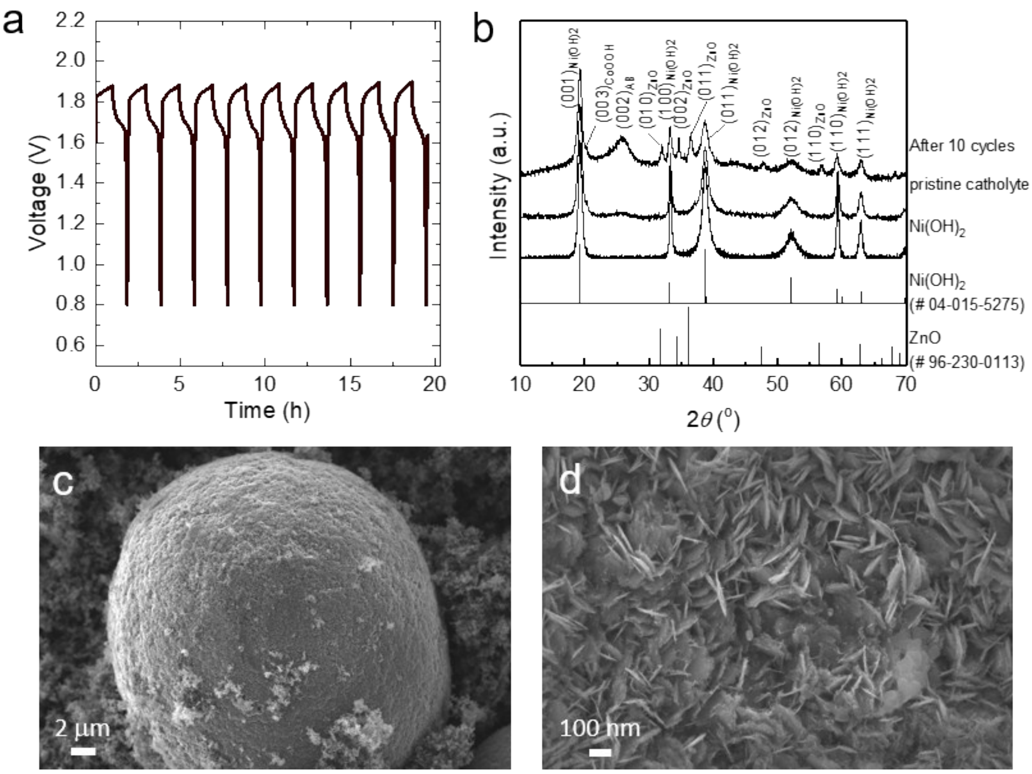

Figure S13. (a) The charge/discharge profiles of Zn-Ni semi-solid static cell containing catholyte with 3.5 vol% $Ni(OH)_2$ + 5.9 vol% AB and 5.2 vol% ZnO + 22.0 vol% Zn anolyte. The applied current was 2 $mA/cm^2_{geo.}$. The charge capacity was limited to 60 % SOC. The above charge/discharge curves were collected after one activation cycle with 120% SOC as described in the experimental section. (b) The XRD patterns of β-$Ni(OH)_2$, the powder collected from pristine $Ni(OH)_2$ catholyte (3.5 vol% $Ni(OH)_2$ and 5.9 vol% AB catholyte) and the powder collected from the catholyte after 10 cycles with current density of 2 mA/cm^2_{geo} in the discharge state. (c) The sphere morphology of β-$Ni(OH)_2$ remained unchanged after 10 cycles (Figure S11a, before cycling) and (d) plate-like particles formed on the spherical particles.

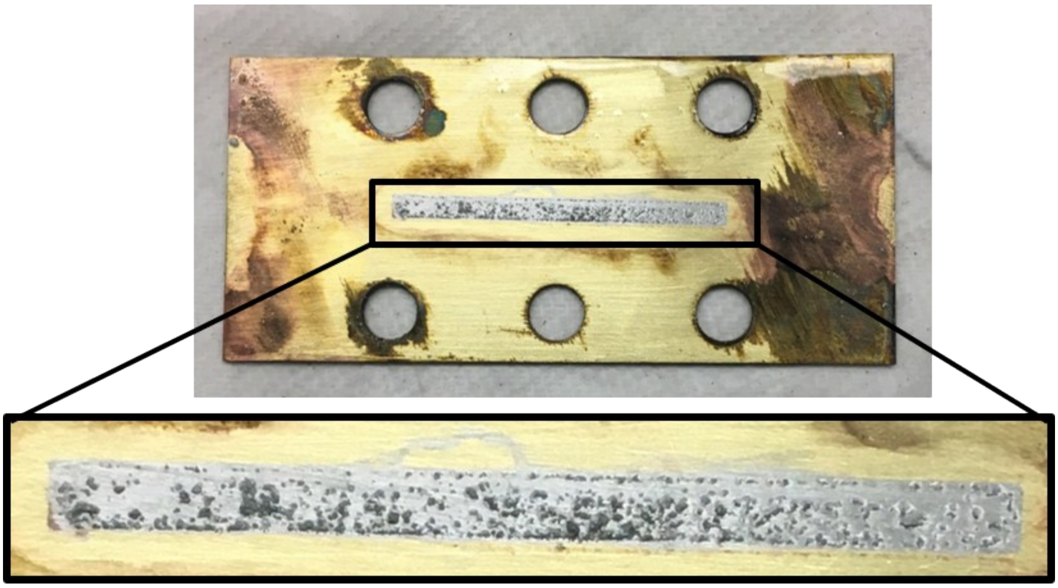

Figure S14. The brass current collector from a semi-solid flow battery after 10 charge-discharge cycles (two batches in Figure 7 in the main text). There are plated Zn particles anchored on the brass surface, which could potentially cause channel blockage.

Generalized Newtonian model fitting for experimental flow curve data

In order to calculate the energy loss due to pumping or to model the flow field in the suspension, it is important to express flow curve data for non-Newtonian suspensions used in this study with generalized Newtonian fluids using constitutive equations such as the Bingham model and Herschel-Bulkley-Papanastasiou model. The shear stress for the Bingham model and the Herschel-Bulkley-Papanastasiou model can be expressed using the following equations[11],

(Bingham model) $$\tau = \tau_y + \mu_p \dot{\gamma}$$

(Herschel-Bulkley-Papanastasiou model; HB-M) $$\tau = \tau_y\left(1 - e^{-m\dot{\gamma}}\right) + k\dot{\gamma}^n$$

where τ is the shear stress, τ_y is the yield stress, μ_p is the plastic viscosity, m is a regularization parameter, k is the fluid consistency, n is the flow index and $\dot{\gamma}$ is the shear rate. In the limit $m \to \infty$ and $n \to 1$, the HBM model approaches the similar limit of the Bingham fluid. The primary advantage of expressing the flow curve in Bingham model is that useful expressions for key design parameters such as energy loss due to pumping or and the expected velocity field in the flowing suspension can be determined analytically. Although the Bingham model does not entirely capture other rheological characteristics of these multiphase complex semi-solid battery slurries such as wall slip or shear-induced migration, it suffices to provide upper-bound approximate expressions for the desired results. In order to capture more advanced 'non-Bingham–like' behavior, the Herschel-Bulkley-Papanastasiou model can be used with numerical simulations of the suspension flow. Interested readers are referred to *Dynamics of Polymeric Liquids*[11] for further information on these models. In the present study, the Bingham model is fitted to the high shear rate region of each measured flow curve (where slip effects are minimal) in order to obtain an upper-bound estimate of the suspension yield stress, which is then used in analytical calculations of the power required for pumping. Wall slip, and the deviation of the measured data below the Bingham asymptote (due to true wall slip or to apparent slip arising from shear-induced migration of suspended particles away from high-shear regions near walls) will only reduce the needed pumping power. The values of the model parameters for each of the suspensions tested in this study are given in Table S1-S4.

Table S5. Fitting parameters for flow curve for 23.1 vol% of Zn suspension (Fig. 3a)

	Bingham model	**Herschel-Bulkley-Papanastatiou model**
Yield stress, τ_y (Pa)	74.8	76.0
Plastic viscosity, μ_p (Pa.s)	0.164	-
Fluid consistency, k (Pa.s^n)	-	0.129
Regularization parameter, m (s)	-	3.1
Flow index, n (-)	-	1.0
Goodness-of-fit, R^2 (-)	1.00	1.00

Table S6. Fitting parameters for flow curve for 6.2 vol% of AB (Fig. 3b)

	Bingham model (above $\dot{\gamma}$ = 45 s^{-1})	**Herschel-Bulkley-Papanastatiou model**
Yield stress, τ_y (Pa)	209	187
Plastic viscosity, μ_p (Pa.s)	0.194	-
Fluid consistency, k (Pa.s^n)	-	0.769
Regularization parameter, m(s)	-	0.4
Flow index, n (-)	-	0.8
Goodness-of-fit, R^2 (-)	0.96	0.95

Table S7. Fitting parameters for flow curve for 22.0 vol% of Zn and 5.2 vol% of ZnO suspension (Fig. 3a)

	Bingham model (above $\dot{\gamma}$ = 100 s^{-1})	**Herschel-Bulkley-Papanastatiou model**
Yield stress, τ_y (Pa)	221	166
Plastic viscosity, μ_p (Pa.s)	0.308	-
Fluid consistency, k (Pa.s^n)	-	4.57
Regularization parameter, m (s)	-	1.7
Flow index, n (-)	-	0.6
Goodness-of-fit, R^2 (-)	0.99	0.99

Table S8. Fitting parameters for flow curve for 5.4 vol% of AB and 12.5 vol% of Ni(OH)2 (Fig. 3b)

	Bingham model (above $\dot{\gamma}$ = 45 s^{-1})	**Herschel-Bulkley-Papanastatiou model**
Yield stress, τ_y (Pa)	203	149

Plastic viscosity, μ_p (Pa.s)	0.163	-
Fluid consistency, k (Pa.s^n)	-	3.21
Regularization parameter, m (s)	-	0.6
Flow index, n (-)	-	0.6
Goodness-of-fit, R^2 (-)	0.96	0.96

References:

1. W. K. Zhang, X. H. Xia, H. Huang, Y. P. Gan, J. B. Wu and J. P. Tu, *Journal of Power Sources*, 2008, **184**, 646-651.
2. H. Parant, G. Muller, T. Le Mercier, J. Tarascon, P. Poulin and A. Colin, *Carbon*, 2017, **119**, 10-20.
3. G. Machell and G. N. Richards, *Journal of the Chemical Society (Resumed)*, 1958, 1199-1204.
4. L. F. Urry, US Pat., US5962163A, 1999.
5. B. J. Hopkins, K. C. Smith, A. H. Slocum and Y.-M. Chiang, *Journal of Power Sources*, 2015, **293**, 1032-1038.
6. F. Y. Fan, W. H. Woodford, Z. Li, N. Baram, K. C. Smith, A. Helal, G. H. McKinley, W. C. Carter and Y.-M. Chiang, *Nano letters*, 2014, **14**, 2210-2218.
7. Z. Li, K. C. Smith, Y. Dong, N. Baram, F. Y. Fan, J. Xie, P. Limthongkul, W. C. Carter and Y.-M. Chiang, *Physical Chemistry Chemical Physics*, 2013, **15**, 15833-15839.
8. J. Piau, *J Non-newton Fluid*, 2007, **144**, 1-29.
9. B. R. Alves and W. D. Cooper, *Journal of the Chemical Society, Faraday Transactions 1: Physical Chemistry in Condensed Phases*, 1981, **77**, 889-896.
10. K. C. Liu and M. A. Anderson, *Journal of The Electrochemical Society*, 1996, **143**, 124-130.
11. R. B. Bird, R. C. Armstrong and O. Hassager, *Dynamics of polymeric liquids. Vol. 1: Fluid mechanics*, 1987.